RSC Advances

PAPER

View Article Online
View Journal | View Issue

Cite this: *RSC Adv.*, 2023, **13**, 21071

Biochar production from cellulose under reductant atmosphere: influence of the total pyrolysis time†

J. L. Santos, * M. A. Centeno and J. A. Odriozola

Received 9th May 2023
Accepted 8th June 2023

DOI: 10.1039/d3ra03093h

rsc.li/rsc-advances

Today's rising energy costs, coupled with increasing energy demand, make it necessary to search for more efficient energy processes. In recent years, there have been increasing efforts to develop efficient catalysts based on waste-derived char, by a single step where the carbon precursor and the metallic active phase one undergo a single common thermal process under a reductant atmosphere at high temperature. The use of a reductant atmosphere drives the formation of carbonaceous materials with different characteristics than those obtained under the standard nitrogen-inert one. Our work evaluates the influence of the residence time and the heating rate on the physicochemical properties of the biochar obtained. Relatively long residence times and slow heating rates, improve the yield to the resulting biochar, without increasing production cost, making the subsequent char-based metallic catalyst synthesis more efficient. The heating rate was shown to be key in improving the properties of the char in a smoother and more controlled way, unlocking a new working pathway for the efficient design and production of char-based catalysts in a one-pot synthesis.

1. Introduction

Biochar is considered a pyrogenic carbon-rich material produced purposefully from waste carbon-neutral sources by controlled pyrolysis.[1] Recently, many efforts have been directed toward demonstrating that char derived from biomass waste has considerable environmental benefits.[2,3] The high robustness of biochars in non-oxidizing atmospheres combined with their mouldable physicochemical properties makes them suitable candidates for many versatile applications in the environmental (greenhouse gas emissions reduction, carbon sequestration, and waste management, *etc.*) and agricultural practices domains (soil amelioration and fertilizer runoff reduction, among others).[4,5]

In addition to these applications, biochar-based materials have shown developed porosity, high thermal stability, and great surface activation, which makes them suitable for catalytic applications, both as supports or catalysts themselves.[6–12] Considering that nowadays 95% of industrial products are obtained through a catalytic process[13] and that this percentage is continuously growing, many efforts are directed towards lessening their production costs and the use of more environmentally friendly materials. One-step processes are a strategy that has been extensively used to reduce production costs in obtaining products derived from residual biomass[14] or in the synthesis of inorganic heterogeneous catalysts.[15,16] Minimizing the preparation procedure to a unique step not only contributes to the lowering of the amount of generated residues and the final energy cost but also efficiently enhanced the development of the circular economy of renewable resources.[17,18] Although some first approaches have been made in recent years to obtain one-stage carbon-based catalysts[19–22] to the best of our knowledge, no work has yet been reported in which residual biomass is used as a carbon precursor to obtaining one-pot catalysts by pyrolysis procedures. The use of residual biomass as a carbon precursor in pyrolytic processes would become biochars an alternative promising alternative to replace conventional solid carbon-based catalysts, giving this type of material a great added value and helping to decrease the wastes production derived from lignocellulosic biomass resources.[23] Another main advantage of the use of biochars is the easy tunability of their physicochemical properties by modifying the main operating parameters of the thermal process.[24] Thus, the fine control of the residence time, temperature, atmosphere, reactor pressure, biomass particle size, and heating rate, plays a fundamental role in optimizing the final product. Typically, slow pyrolysis has been studied in an inert or oxidizing atmosphere (N_2, He, Ar, CO_2, CO, H_2O, *etc.*), however, it has recently been demonstrated that the thermal decomposition process in a reductant atmosphere could facilitate the direct obtaining of the activated char-catalysts in a one-pot step, altering the properties of the biochar compared to those of the biochar produced under inert or oxidant ones.[21,22,24] Although the influence of some important parameters of the pyrolysis process under hydrogen atmosphere, such as temperature, have been previously reported.[24,25]

Instituto de Ciencias de Materiales de Sevilla, Centro Mixto CSIC-Universidad de Sevilla, Avda, Américo Vespucio 49, 41092 Seville, Spain. E-mail: josel.santos@icmse.csic.es

† Electronic supplementary information (ESI) available. See DOI: https://doi.org/10.1039/d3ra03093h

There is still a great lack of knowledge on how the other decisive pyrolysis parameters, such as the total pyrolysis time or heating rate, affect the properties or even the yield of the resulting char-based material.[26] This lack, together with the uncertainty induced by the presence of metal functionalities, makes up to know, the one-pot synthesis of metal-biochar catalysts a not-very-used method.

In the present work, we will at least partially cover this lack, with the study of the microcrystalline cellulose (as representative of biomass) pyrolysis process in a model reductant atmosphere (N_2/H_2 1 : 1 mixture), focusing on the influence of total pyrolysis time. Residence time and heating rate were modified, to analyze the char yields as well as on physicochemical properties of the obtained materials. Slow pyrolysis parameters were sought where the performance towards the solid fraction was favored.[27,28] According to our previous study,[24] it was decided to work in a typical slow pyrolysis condition. Fixed intermediate pyrolysis temperature (700 °C), long residence times, from 1 minute to 4 hours, and slow heating rate, from 5 °C min^{-1} to 20 °C min^{-1}.

2. Experimental

2.1 Materials

Commercial fine powder (75–250 μm particle size) microcrystalline cellulose was purchased by Alfa Aesar®. Moisture content was calculated in a 5 wt% and the proximate analysis determined to be a nitrogen and sulphur-free material, composed of carbon (42.7 wt%), hydrogen (6.2 wt%) and oxygen (51 wt%).

2.2 Heat treatment: pyrolysis

Commercial cellulose was pyrolyzed in a bed configuration steel tube reactor (≈687 cm^3) placed in a cylindrical oven with a horizontal opening, as shown in Fig. S1.† About 50 g. of cellulose was loaded in an alumina boat at room temperature and the reactor was purged with nitrogen for 10 min. Then, the flow rate of a reductant mixture (N_2/H_2, 1 : 1 volume ratio) was set to 200 mL min^{-1} with mass flow controllers (Bronkhorst brand, High-Tech model). After 30 min stabilization, the temperature, controlled with a type-K thermocouple located in contact with the external wall of the reactor, was increased up to 700 °C at the selected constant heating rate (5, 10, or 20 °C min^{-1}). Once the temperature was achieved, several residence times were evaluated (1, 120, and 240 min). After this time, the heating was stopped, and the reactor was allowed to cool to room temperature in the reactant atmosphere. The liquid fraction was collected in a cold trap placed in an ice bucket, and the gas fraction was released into the atmosphere. The char yield was calculated by difference and the estimated error was less than ±1.0%.

As shown in Table 1, five materials were prepared and labelled as $C_{t,R}$, where C is char, t is the residence time, 1–240 (min), and R is the heating rate, 5–20 (°C min^{-1}).

2.3 Characterization techniques

Prepared biochar was deeply characterized according to the following procedures and techniques:

The proximate analysis for the compositional estimation based on volatile matter, moisture, fixed carbon, and ash, was carried out following the standardized procedures: D3175 for volatile matter,[29] ASTM D3173 for moisture,[30] and D3174 for ash.[31] In addition, the elemental analysis was performed in a CHNS/O analyzer (Leco Truspec® Micro) at a high temperature (1300 °C), using a fixed load sample of 2 mg. In this test, oxygen was estimated by the difference.

X-ray diffractograms (XRD, hereinafter) were obtained in an X'Pert Pro PANalytical diffractometer equipped with a Cu anode and acquired at RT, working in a continuous scan mode (from 2θ 10 to 90°, 0.05° and 300 s per step). The results were compared with the database PDF2 ICDD2000. The char structure parameters, such as crystallite diameter along basal planes (L_a), average stacking height (L_c), and R-value were determined following the approach of Alexander *et al.*[32]

The average stacking height and crystallite diameter of the aromatic carbon sheets were determined using the empirical Scherrer equation, eqn (1) and (2).

$$L_c = \frac{(k_c\lambda)}{(\beta_{002}\cos\theta_{002})} \quad (1)$$

$$L_a = \frac{(k_c\lambda)}{(\beta_{100}\cos\theta_{100})} \quad (2)$$

where k_c is a constant depending on the X-ray reflection plane (0.89 for the (002) peak and 1.84 for the (100) peak); λ is the wavelength of incident X-ray (1.5405 Å for copper K_α radiation); β is the full width at half maximum of the corresponding peak and θ is the peak position. The empirical R-value was defined as the intensity's ratio between the background and the most intense point at the same scattering angle of the (002) peak.[33–35]

Raman spectra were collected using a 532.14 nm green laser, at 5 mW working power, with a 600 grooves per mm diffraction grating and a 50× objective with a confocal aperture of 1000 microns, on an HR800 Horiba Jobin Yvon dispersive microscope.

The Diffuse Reflectance Infrared Fourier Transform Spectroscopy spectra (DRIFTS, hereinafter) were collected at RT with pure samples, after accumulation of 100 scans at 4 cm^{-1} resolution, on a JASCO FTIR 6200 spectrometer equipped with a DRIFTS Pike accessory model EASI-DIFF.

The textural properties of solids were measured by nitrogen isotherms at 77 K in Micromeritics Tristar II equipment. The BET method was applied to obtain the specific surface area (S_{BET}), while for the average pore size (D_{mean}) and pore volume (V_{BJH}), the BJH method was used. Samples were previously degassed at 350 °C for 12 hours using a vacuum degasser system 061 VacPrep Micromeritics.

Thermogravimetric DTA/TG analysis was achieved on a TA Instruments Q600 setup. Samples were heated to 10 °C min^{-1} under synthetic air (100 mL min^{-1}) from RT to 900 °C.

The char's acidity was determined by the stabilized pH of a slurry of the solids in distilled water. The measurements were carried out in a pH-electrode (Metrohm), testing 50 mg of the sample dispersed in 50 ml of distilled water. The resulting

Table 1 Char label and pyrolysis conditions

Sample	Temperature (°C)	Residence time (min)	Heating rate (°C min^{-1})	Total pyrolysis time[a] (min)
$C_{1,10}$	700	1	10	71
$C_{120,10}$	700	120	10	190
$C_{240,10}$	700	240	10	310
$C_{120,5}$	700	120	5	260
$C_{120,20}$	700	120	20	155

[a] Calculated as the time it takes to reach the final temperature added to the residence time of each experiment.

suspension was stirred at a constant speed during the measurement until a fixed pH was reached.[36]

The X-ray photoelectron spectroscopy (XPS) was carried out on a Leybold-Heraeus LHS-1020 with an EA200 detector. The individual XPS spectra were collected at RT, with a constant step energy of 35 eV, 6 min of acquisition time, and a 0.1 eV of the resolution, using a monochromatic Al radiation K_α (30 mA, 11 kV, and 1486.6 eV) and the binding energy was calibrated for the carbon (C1s, at 284.6 eV) with an uncertainty of ± 0.2 eV. General spectra were collected using a resolution of 1 eV, a step energy of 40 eV, and an acquisition time of nine minutes.

The results were processed in the CasaXPS program, using a Shirley baseline for the deconvolution of the spectra. The C (1s) level was fitted according to Lerf–Klinowski's model[37] and the O (1s) level was fitted following Fan *et al.* model.[38]

3. Results and discussion

Char yield and proximate analysis results of the generated biochars are described in Table S1.† In general, the increase in the total pyrolysis time (lower heating rate and longer residence time), affects carbon yield negatively, increasing the liquid and gaseous fractions. The easier thermal cracking of heavy hydrocarbon at long pyrolysis time causes a decrease in the moisture content, resulting in biochar with less volatile matter and a remarkably higher percentage of carbon fixed, clear benefits for their use as catalytic support.[39–41]

As shown in Fig. 1, residence time modifications cause a greater change in the proximate analysis and char yield than alterations done with the heating rate.

The elemental compositions of chars obtained at the different conditions are shown in Table S2.† Typically, an increase in the total pyrolysis time, exemplified in residence time and heating rates, causes a rise in the carbon content and, more remarkably, a drop in the oxygen percentage, Fig. 2. These observations suggest that increasing the total pyrolysis time, by increasing the residence time at the final temperature, or by increasing the time needed to arrive at such temperature, leads toward more aliphatic and graphitic chars, favoring both depolymerization/cleavage and deoxygenation reactions.

A different behavior is visualized for the hydrogen content of the char. Due to the reductant atmosphere, longer pyrolysis times at medium temperatures (700 °C) favor the hydrogenation reactions, resulting in higher H/C ratios and producing less condensed aromatic chars. On the other hand, using lower heating rates allows more complete dehydration of the cellulose by decreasing the time at high temperatures and prolonging the pyrolysis time in the low-temperature range. Similar behavior for the heating rate in the char properties under a nitrogen atmosphere has also been previously described by Brunner *et al.*[42]

The H/C ratios of all obtained chars are in good agreement with those previously presented in the van Krevelen diagram of cellulose char.[43] All these results evidence that pyrolysis time must be taken into consideration for the final design of a catalyst or catalyst support since the aromaticity degree of the carbon obtained can influence the active phase dispersion, the surface acidity, or even the catalytic behavior.[24]

Another important factor to be considered in the design of chars for catalytic applications is their textural properties. It is well known that one of the great advantages of chars in their use as catalytic support is their high specific surface area, which allows them to obtain high metal dispersions increasing the metal surface enrichment and thus the number of available active centers.[44]

Fig. S2† displays the adsorption and desorption isotherms of the resulting chars. All generated chars exhibit type I isotherms, characteristics of mostly microporous materials, with microporosity percentages above 85% in all cases, Table 2.

The results suggest that the specific surface area and the percentage of microporosity of the char increases, to the detriment of pore size with increasing total pyrolysis time, Fig. 3a.

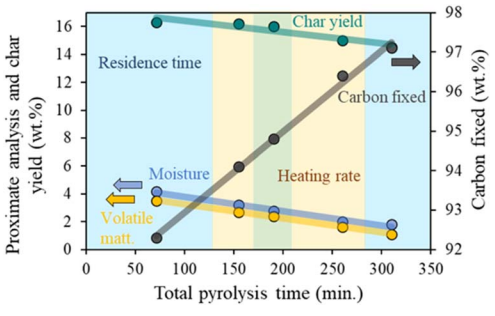

Fig. 1 Influence of total pyrolysis time on proximate analysis, char yield, and carbon fixed (residence time shown in central and outer points, blue zone, and heating rate exhibited in inner points on the graph, orange zone). Although both zones, will not be colored hereinafter, the correlation will be the same.

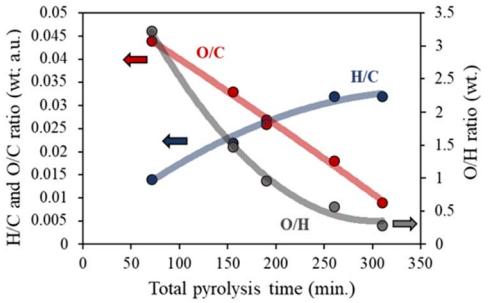

Fig. 2 Impact of the total pyrolysis time (heating rate and residence time) on the compositional ratio of the chars.

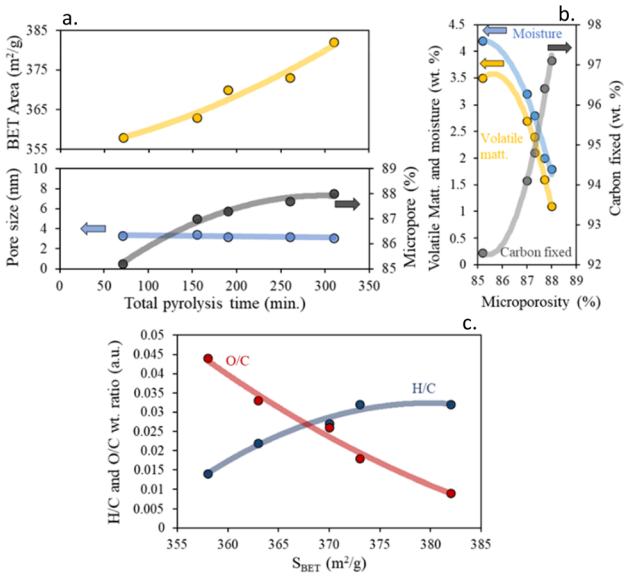

Fig. 3 (a) Impact of total pyrolysis time on textural properties, (b) influence of proximate composition on char microporosity percentage and (c) effect of H/C and O/C wt ratios on BET surface area.

According to the microporosity, an inverse relationship was found for the percentage of moisture and volatile matter. On the contrary, a direct relationship was found with the percentage of fixed carbon. This suggests that the loss of volatile matter with increasing pyrolysis time leads to the formation of microporous chars, due to the reduction of defects between the carbon layers, and to obtaining highly hydrophobic chars, decreasing the percentage of moisture, Fig. 3b.

Consequently, it is possible to have control over the textural properties by controlling the heating rate and residence time of the pyrolysis process. Like the trend found so far, we can determine that residence time has a greater impact on the char textural properties than the heating rate. In addition to that, a clear dependence between the surface area and the aromaticity was found in Fig. 3c. It was found that chars with higher specific surface areas were mostly less aromatic and activated than those with lower specific surface areas.

Williams *et al.*[45] reported a similar dependence on the S_{BET} values of the char produced from the pyrolysis of scrap automotive tires. These textural enhancements are directly derived from the changes in aromaticity, as derived before from the elemental composition of the chars, and can be due to the generation of less aromatic and less functionalized chars. These results are also in agreement with those obtained by Kaminsky *et al.*[46] for microporous char precedent of slow pyrolysis of biomass.

Another important point in the production of chars for catalyst support applications is their robustness and thermal stability, which was evaluated by the derivative of the weight loss. Since the raw material was ash-free microcrystalline cellulose, a complete weight loss was achieved at the end of the measurement.

Fig. S3† presents the DTA/TG curves for the resulting chars under an oxygen atmosphere. In each char, two main processes of weight loss are easily visible. The weight loss at around 50 °C, is related to the desorption of physisorbed water, and the larger weight loss between 300 and 600 °C, is associated with the carbon skeleton combustion.[24] The first process involves a 3–5 wt% loss and indicates a similar moisture capacity of the chars, derived from their similar textural properties. The influence of the pyrolysis residence time in the temperature at which the carbon material obtained is combusted is higher ($\Delta T \approx 50$ °C) than that produced when changing the pyrolysis heating rate, which is indeed small, although significant ($\Delta T \approx 30$ °C), supporting the results found above. Generally, an increment in total pyrolysis time, results in a more stable char with higher carbon fixed content, due to the elimination of secondary reactions and volatiles, resulting in a decrease in carbon yield. This is interesting for the possible application of the material in high-temperature processes in oxidant atmospheres, such as several industrial catalytic reactions on environmental and energetic interests.[47] One could increase the thermal stability of the produced solid in such conditions just by increasing the total pyrolysis time of production. In

Table 2 Textural properties, combustion temperature, and pH of the slurry of chars

Sample	S_{BET} ($m^2\ g^{-1}$)	Ext. area ($m^2\ g^{-1}$)	Microp. (%)	V_{BHJ} ($cm^3\ g^{-1}$)	D_{mean} (4V/A) (nm)	Comb temp. (°C)	pH slurry (a.u.)
$C_{1,10}$	358	53	85.2	0.023	1.8	525	5.4
$C_{120,10}$	370	47	87.3	0.019	1.7	550	5.6
$C_{240,10}$	382	46	88.0	0.019	1.6	575	5.7
$C_{120,5}$	373	46	87.7	0.021	1.7	565	5.6
$C_{120,20}$	353	46	87.0	0.019	1.9	537	5.5

particular, the increment of the residence time and/or the decrease of the heating rate, results in a more orderly, less amorphous char with a higher combustion point, Fig. 4b. In good agreement with the literature under an inert atmosphere, a decrease in the aromatic character of the chars, (low H/C ratios), results in an increase in thermal stability,[48] which is very attractive for use in catalytic applications requiring medium or high temperatures. However, higher thermal stability results in lower surface functionalization of the char, which will cause an increase in char crystallinity, resulting in more hydrophobic chars.[49]

Generally, it is well known that char stability depends on its properties, such as crystallinity and graphitization, among others.[50] Thus, the degree of graphitization and crystallinity of the samples were studied by X-ray diffraction, Fig. S4.†

X-ray diffractograms of the resulted chars exhibit three broad characteristic peaks of amorphous chars at $2\theta \approx 23$, 44, and 80°, ascribed to (002), (100), and (110) planes, respectively.[7,10,24] It is well known that the (002) peak is attributed to the stacking structure of graphene layers, while the (100) and (110) bands are related to the in-plane graphene structure. In addition, the intensity, position, and full width at half maximum of those peaks are directly correlated with the crystallinity grade, crystal size, and shape.[34,51]

Fig. S4† shows that the residence time constitutes a key factor in the crystallinity of the chars obtained by slow pyrolysis. In general, when pyrolysis time increased further, XRD peaks narrowed and became more intense, indicating a progressive rearrangement of the graphene sheets, which resulted in the formation of bigger crystallites.[52] In this sense, it was found that an increase in the pyrolysis time at the same temperature (700 °C) caused an increase in the crystallinity of the solid obtained or, what is the same, a decrease in the amorphousness of the resulting char, indicating an improvement in the structural ordering of the short-term char.

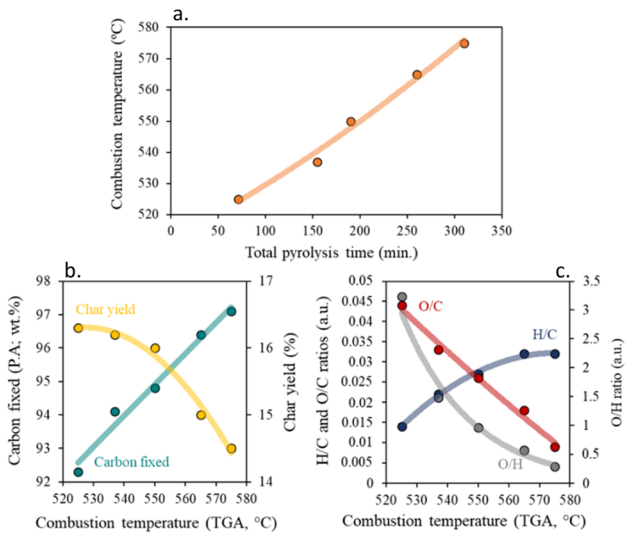

Fig. 4 Impact of total pyrolysis time on (a) combustion temperature and influence of combustion temperature on (b) carbon fixed and char yield, and (c) H/C, O/C and O/H ratios.

The heating rate does a more damped influence on the generated char, obtaining very similar XRD diffraction patterns for the three tested heating rates (5, 10, and 20 °C min^{-1}). In all cases, defined bands are obtained, indicating a short-term ordering of the carbon structure obtained. Based on eqn (1) and (2), the values of the structural parameters were calculated for all obtained chars, and the results are summarized in Table 3.

As seen in the diffraction pattern, any pyrolysis parameter leading to less amorphous carbon, such as increased total pyrolysis time, leads to higher L_a, L_c, and R parameters. As previously described,[45,46] the enhancements of textural properties directly derive from the modification of the short-term order of the carbon layers, Fig. 5b. Thus, a decrease in the short-term order, (lower values of L_a and L_c), results in chars with more graphene-like properties (lower values of packing factor, R-value) and poorer textural properties. By contrast, chars with higher short-term order (more graphitic character) showed packing values closer to 2 and a higher specific surface area.

In a deeper analysis of the crystallinity of the obtained chars, their Raman spectra were analyzed, Fig. S5.† It has generally been described that an increase in the disorder of the graphite structure results in an increase in the relative intensity of the D-band.

However, in amorphous chars, an increase in the intensity D/G band ratio can indicate an increase in the crystallinity of the generated chars.[53] However, the parameters of the Raman spectrum and their correlation with the degree of graphitization of the solid have been determined in different ways, which makes it very difficult to compare the results and greatly limits the completeness of the conclusions obtained.[54] From the various parameters proposed as indicative of graphitization level in the Raman spectrum of chars, the ratio of D/G band intensities (in any of its two analogous forms) is the most used.

Fig. S5b† shows that bands of the Raman spectra of chars sharpen up with increasing the total pyrolysis time, indicating the ordering in the carbon structure, Fig. 6a. The variations of I_D/I_G also result from the growth of stacking graphene layer and the loss of structural defects and imperfections acting as active sites, Fig. 6b.

However, derived from the similarity of Raman spectra, the heating rate reduction has a milder effect compared to the lengthening of the residence time at high temperatures.

Another key factor in catalytic support preparation, is their surface chemistry, since the metal support anchoring is done through oxygenated groups. For this purpose, the surface chemistry of the resulted chars was evaluated by DRIFTS, and the results are shown in Fig. S6.†

In general terms, the small absorption band located at 3030–3050 cm^{-1} is assigned to aromatic C–H stretching, while the aliphatic C–H stretching appears in the 2920–2850 cm^{-1} region, with the CH_2 group being the main contributor.[55]

As can be seen, at low total pyrolysis times, the intensity of the aromatic C–H stretching is significantly greater than the aliphatic C–H ones, suggesting that aromatic chars can be

Table 3 Atomic surface composition (XPS), bulk composition (elemental analysis), structural parameters (XRD), and I_D/I_G ratio calculated by Raman

	Surface (% at; XPS)			Bulk (% at; E.A.)			Structure (XRD)			Raman
Sample	C	O	O/C	C	O	O/C	L_a (Å)	L_c (Å)	R (Å)	I_D/I_G (a.u.)
$C_{1,10}$	91.3	8.7	0.096	94.4	4.2	0.044	20	15	1.33	0.806
$C_{120,10}$	94.4	5.6	0.059	94.8	2.5	0.026	22	15	1.71	0.884
$C_{240,10}$	97.3	2.7	0.028	95.9	0.9	0.009	26	17	1.85	0.905
$C_{120,5}$	95.2	4.8	0.051	95.2	1.7	0.018	25	15	1.75	0.901
$C_{120,20}$	93.5	6.5	0.070	94.3	3.1	0.033	18	14	1.65	0.866

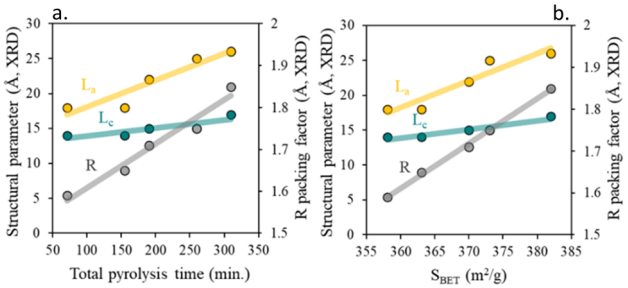

Fig. 5 (a) Influence of total pyrolysis time on char structural parameters and (b) impact of total surface area on char structural parameter.

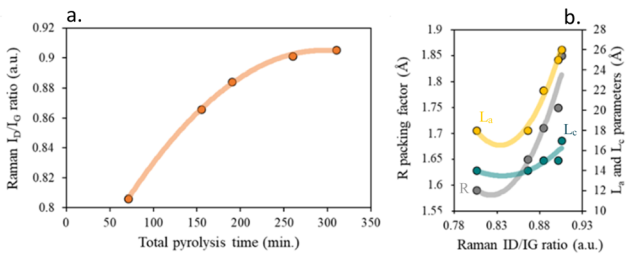

Fig. 6 (a) Effect of pyrolysis time on the crystallinity of chars based on Raman I_D/I_G band ratios and (b) impact of Raman I_D/I_G ratio on the distance between carbon layers.

obtained under these working conditions, as previously proposed (Fig. 7).[24]

An increment in the pyrolysis time (increase in the residence time and/or decrease in heating rates) leads to a decrease in the aromatic char's proportion.

On the other hand, the weak band observed at 1727 cm^{-1} in the samples obtained at low residence times and high heating rates, Fig. S6e,† corresponds to residual moisture.[56] The absence of this band in the other samples indicates the low percentage of moisture contained in such samples, as evidenced in the proximate analysis, Table S1.† The small shoulder at ≈1700 cm^{-1} is attributed to the presence of carbonyl groups,[56] suggesting a surface functionalization in the chars, which progressively decreases with increasing residence time and decreasing heating rate.

The band at 1600 cm^{-1} is assigned to polyaromatic systems and benzene rings.[57] In addition, the weak band at 1500 cm^{-1} is usually attributed to C=C bonds in benzene rings.[55] In general terms, the bands at 1450–1440 cm^{-1} and 1380–1375 cm^{-1} have been correlated with aliphatic bending modes, and that of 1261–1150 cm^{-1} is attributed to C–O single bond stretching, due to the, mostly presence of ethers and alcohols.[58] Finally, the bands between 900 and 700 cm^{-1} correspond to aromatic bending modes and are mainly due to aromatic HCC (hydrogen–carbon–carbon) rocking vibrations in aromatic and condensed aromatic ring systems.[59]

From DRIFTS analysis, it is evident that the surface functionalization degree and the consequent hydrophobic-hydrophilic character are also dependent on the pyrolysis conditions, and it is expected that an increase in the surface functionalization led to an increment in the surface acidity and the hydrophilicity character which will improve its subsequent dispersion in aqueous media.

For the evaluation of surface acidity, the pH at which the slurry of the solids is stabilized in water was measured, and the results are shown in Fig. S7.†

Although all obtained chars have a slightly acidic surface, a loss of surface acidity is observed with the increase of the residence time. Meanwhile, for the heating rate, the increase of the pH of the media is weaker with the decrease in the heating rate (Fig. 8).

The surface functional groups' nature was further characterized by X-ray photoelectron spectroscopy and the general spectrum of solids is presented in Fig. S8.† The XPS quantitative analysis of the elements reveals a similar surface atomic composition to bulk ones determined by elemental analysis, pointing to a high homogenization degree of carbon particles, Table 3.

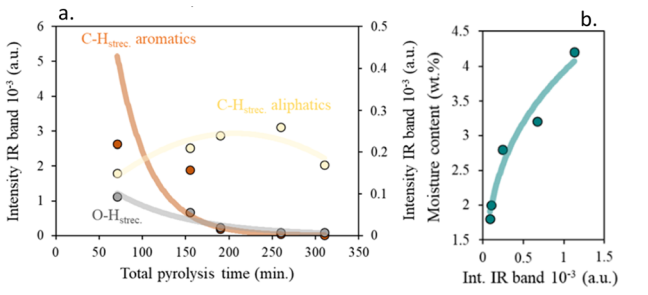

Fig. 7 (a) Effect of total pyrolysis time on surface char activation and (b) impact of surface char activation on physisorbed water.

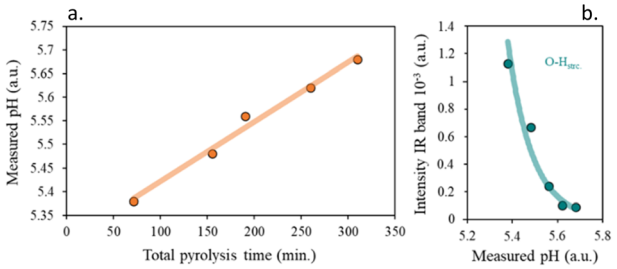

Fig. 8 (a) Impact of the total pyrolysis time on measured pH and (b) on char surface activation.

Table 3 evidence that the surface of the resulting chars loses density of oxygenated groups in the surface with the increase of the residence time, remaining almost constant with the heating rate. On the other hand, and in comparison, with the bulk atomic composition calculated by elemental analysis, higher percentages of oxygen and higher atomic O/C ratios were found at the surface, indicating a higher surface functionalization than mass.

A good fitting was found for the surface functionalization and the pH of the char slurry, confirming that the char acidity is directly proportional to the oxygen surface content, Fig. 9b. It is clearly visible, that, as expected, an increase in the functional groups content, led to more acidic chars.

The analysis of the spectra for the C (1s) and O (1s) levels is shown in Fig. S9.† The spectrum corresponding to the C (1s) level was deconvolved into four signals ascribed to the C=C species of the aromatic rings (at 284.6 eV, dark red), hydroxyl species (C–OH, at 285.8 eV, orange), carbonyl species (C=O, at 287.2 eV, brown) and carboxyl groups (–COOH, at 288.5 eV, dark blue), respectively. The analysis of the energy level corresponding to O (1s) was performed by deconvolution of the spectrum into three signals: the orange one at 530.2 eV attributed to hydroxylic species, a second one at 532 eV (dark blue) assigned to carbonyl groups; and the third one at 533.5 eV (dark red) associated to physisorbed water (hydrophilic character).[60]

An increase in residence time causes a rise in the relative population of sp^2 carbon character, indicating an increase in the aromatic character and a drop in the functionalization degree of the char surface. This would explain the decrease in surface acidity and functionalization and the resulting hydrophilic character found in these samples. However, the XPS spectra of the chars obtained at different heating rates are quite like each other, with small differences in the surface functional groups' proportion. In addition, the increase of the heating rate enhanced the hydrophilicity of the resulting char, as was previously demonstrated[61] and evidenced by the results of elemental analysis in Table S2.† Therefore, the surface analysis performed by XPS confirms for the heating rate the same trend found for the residence time with a more diluted impact on final properties.

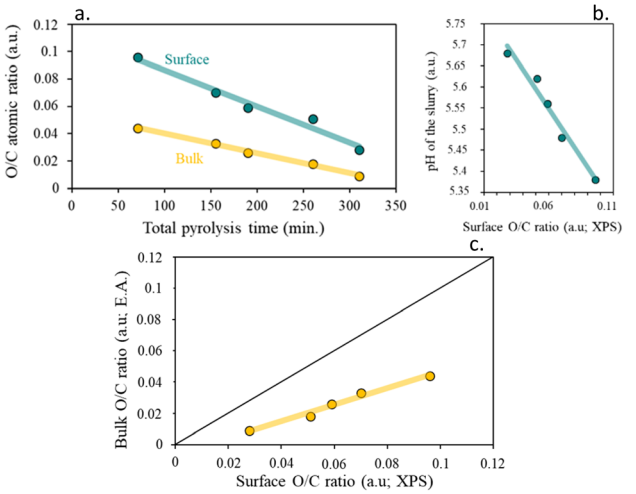

Fig. 9 (a) Impact of total pyrolysis time on O/C atomic ratio, (b) influence of surface O/C ratio on pH of the slurry (IEP) and (c) surface O/C ratio (XPS) correlation.

4. Conclusions

In the current work, slow pyrolysis of commercial cellulose under a reductant atmosphere was performed to investigate the influence of the total pyrolysis time, in terms of residence time and heating rate, on char physicochemical properties. The development of desired textural properties, surface chemical activation, thermal stability, and final carbon yield becomes key factor in the development of one-pot char-based catalysts.

An increase in residence time above two hours leads to an impoverishment of char surface chemical activation. This could result in a significant reduction of the metal-char anchor bonds, leading to poor dispersion of the active phase in the resulting catalyst. However, the use of very short residence times would result in chars with a lower specific surface area and thermal stability, which would reduce their subsequent applications and hinder the metallic dispersion of the subsequent one-pot catalyst. On the other hand, using very high heating rates results in biochars with adequate surface functionalization, average specific surface areas, and high char yields. On the contrary, decreasing the heating rate during pyrolysis would lead to the loss of final char and a decrease of surface chemistry, which would hinder further dispersion of the active phase.

In general terms, it was found that the heating rate had a more attenuated impact than the residence time does on the physicochemical properties of the biochar. Thus, in the synthesis of one-pot char-based catalysts, the use of the heating rate will be proposed to dampen the catalytic impact of the presence of metals during the pyrolysis process.

In summary, it could be concluded that is possible to modulate the surface and physicochemical properties of char through the residence time and the heating rate, as a prior approach in the synthesis of char-based catalysts in one-pot pyrolysis treatment under reductant atmospheres.

Conflicts of interest

The authors declare that they have no known competing financial interests or personal relationships that could influence the work reported in this paper.

Acknowledgements

Financial support for this work was obtained from Spanish Ministerio de Ciencia e Innovación (MCIN/AEI(10.13039/501100011033)/FEDER Funds una manera de hacer Europa), Project PID2020-113809RB-C32 and Junta de Andalucía *via* Consejería de Transformación Económica, Industria, Conocimiento y Universidades and its PAIDI 2020 program (Grant: P18-RT-3405) all co-financed by FEDER funds from the European Union.

References

1 J. Lee, K.-H. Kim and E. E. Kwon, *Renewable Sustainable Energy Rev.*, 2017, **77**, 70–79.
2 O. Abiola Fakayode, H. Wahia, L. Zhang, C. Zhou and H. Ma, *Fuel*, 2023, **332**, 126071.
3 M. Inyang and E. Dickenson, *Chemosphere*, 2015, **134**, 232–240.
4 J. Lehmann, J. Gaunt and M. Rondon, *Mitigation and Adaptation Strategies for Global Change*, 2006, vol. 11, p. 403.
5 J. Lehmann and S. Joseph, *Biochar for environmental management: an introduction*, Earthscan, London, 2009, p. 1.
6 P. Serp and J. L. Figueredo, *Carbon materials for catalysis*, John Wiley & Sons, Inc., 2009.
7 C. Megías-Sayago, J. L. Santos, F. Ammari, M. Chenouf, S. Ivanova, M. A. Centeno and J. A. Odriozola, *Catal. Today*, 2018, **306**, 183–190.
8 J. L. Santos, M. Alda-Onggar, V. Fedorov, M. Peurla, K. Eränen, P. Mäki-Arvela, M. Á. Centeno and D. Yu. Murzin, *Appl. Catal., A*, 2018, **561**, 137–149.
9 J. L. Santos, L. F. Bobadilla, M. A. Centeno and J. A. Odriozola, *C*, 2018, **4**, 47–63.
10 H. Rodriguez Molina, J. L. Santos, M. I. Domínguez Leal, T. R. Reina, S. Ivanova, M. A. Centeno and J. A. Odriozola, *Front. Chem.*, 2019, **7**, 548–561.
11 J. L. Santos, C. Leon, G. Monnier, S. Ivanova, M. A. Centeno and J. A. Odriozola, *Int. J. Hydrogen Energy*, 2020, **45**, 23056–23068.
12 E. Auer, A. Freund, J. Pietsch and T. Tacke, *Appl. Catal., A*, 1998, **173**, 259–271.
13 B. J. O'Neill, D. H. K. Jackson, J. Lee, C. Canlas, P. C. Stair and C. L. Marshall, *ACS Catal.*, 2015, **5**, 1804–1825.
14 S. Shao, Z. Ye, X. Hu, J. Sun, X. Li and H. Zhang, *Fuel*, 2023, **333**, 126238.
15 D. H. Kim, *Catal. Today*, 2015, **256**, 130–136.
16 Q. C. Do, Y. Kim, T. An Le, G. J. Kim, J.-R. Kim, T.-W. Kim, Y.-J. Lee and H.-J. Chae, *Appl. Catal., B*, 2022, **307**, 121167.
17 Y. Chen, T. Zhang and Q. Liu, *Int. J. Hydrogen Energy*, 2021, **46**, 30373–30381.
18 C. Zhou, C. Fasel, R. Ishikawa, M. Gallei, Y. Ikuhara, S. Lauterbach, H.-J. Kleebe, R. Riedel and E. Ionescu, *J. Eur. Ceram. Soc.*, 2017, **37**, 5193–5203.
19 X. Zhuang, K. Jin, Q. Zhang, J. Liu, X. Zhang, H. Zhan and L. Ma, *Chin. Chem. Lett.*, 2022, **33**(5), 3–26.
20 F. Cazaña, A. Galetti, C. Meyer, V. Sebastian, M. A. Centeno, E. Romeo and A. Monzón, *Catal. Today*, 2018, **301**, 226–238.
21 C. Cao, L. Wei, M. Su, G. Wang and J. Shen, *Carbon*, 2017, **112**, 27–36.
22 Z. Xiao, Q. Ge, C. Xing, S. Fang, J. Ji and J. Mao, *J. Fuel Chem. Technol.*, 2015, **43**, 1446–1453.
23 A. Demirbas and G. Arin, *Energy Sources*, 2002, **24**, 471–482.
24 J. L. Santos, M. A. Centeno and J. A. Odriozola, *J. Anal. Appl. Pyrolysis*, 2020, **148**, 104821–104832.
25 A. Downie, A. Crosky and P. Munroe, *Biochar for environmental management–science and technology*, Earthscan Publications, London, 2009, pp. 13–32.
26 P. Roy and G. Dias, *Renewable Sustainable Energy Rev.*, 2017, **77**, 59–66.
27 C. K. and O. Mašek, *Bioresour. Technol.*, 2014, **162**, 148–156.
28 K. S., F. Zehetner, A. Dellantonio, R. Hamid, F. Ottner and V. Liedtke, *J. Environ. Qual.*, 2012, **41**, 990–1000.
29 ASTM D 3175-02, Annual book of ASTM standards, Test method for volatile matter in the analysis sample of coal and coke, Gaseous Fuels: Coal Coke, 2005, 05.06.
30 ASTM D 3173-03, Annual book of ASTM standards, Test method for moisture in the analysis sample of coal and coke, Gaseous Fuels: Coal Coke, 2005, 05.06.
31 ASTM D 3174-04, Annual book of ASTM standards, Test method for ash in the analysis sample of coal and coke from coal, Gaseous Fuels: Coal Coke, 2005, 05.06.
32 L. E. Alexander and E. C. Sommer, *J. Phys. Chem.*, 1956, **60**, 1646–1649.
33 G. N. Okolo, W. J. P. Neomagus, C. Everson, J. Roberts, R. Bunt, R. Sakurovs and P. Mathews, *Fuel*, 2015, **158**, 779–792.
34 J. Collins, D. Zheng, K. Ngo, D. Qu and M. Foster, *Carbon*, 2014, **79**, 500–517.
35 Y. Liu, J. S. Xue, T. Zheng and J. R. Dahn, *Carbon*, 1996, **34**, 193–200.
36 H. Markus, P. Mäki-Arvela, N. Kumar, N. V. Kulkova, P. Eklund, R. Sjöholm, B. Holmbom, T. Salmi and D. Yu Murzin, *Catal. Lett.*, 2005, **103**, 1–2.
37 H. He, J. Klinowski, M. Forster and A. Lerf, *Phys. Lett.*, 1998, **287**, 53–56.
38 X. Fan, C. Yu, J. Yang, Z. Ling and J. Qiu, *Carbon*, 2014, **70**, 130–141.
39 J. H. Windeatt, A. B. Ross, P. T. Williams, P. M. Forster, M. A. Nahil and S. Singh, *J. Environ. Manage.*, 2014, **146**, 189.
40 A. Cross and S. P. Sohi, *GCB Bioenergy*, 2013, **5**, 215.
41 H. Y. Zhang, R. Xiao, D. H. Wang, G. Y. He, S. S. Shao, J. B. Zhang and Z. Zhong, *Bioresour. Technol.*, 2011, **102**, 4258–4264.
42 P. H. Brunner and P. V. Roberts, *Carbon*, 1980, **18**, 217–224.
43 X. Cao, S. Sun and R. Sun, *RSC Adv.*, 2017, **7**, 48793–48805.
44 J. L. Santos, L. M. Sanz-Moral, A. Aho, S. Ivanova, D. Yu Murzin and M. A. Centeno, *Biomass Bioenergy*, 2022, **163**, 106504.
45 P. T. Williams, S. Besler and D. T. Taylor, *Fuel*, 1990, **69**, 1474–1482.
46 W. Kaminsky, C. Mennerich and Z. Zhang, *J. Anal. Appl. Pyrolysis*, 2009, **85**, 334–337.
47 C. Tian, L. Yuan, T. Wen, E. Jin, D. Jia and J. Yu, *Ceram. Int.*, 2020, **46**(6), 7871–7878.

48 P. Morf, P. Hasler and T. Nussbaumer, *Fuel*, 2002, **81**, 843–853.
49 N. Gao, F. Wang, C. Quan, L. Santamaria, G. Lopez and P. T. Williams, *Prog. Energy Combust. Sci.*, 2022, **93**, 101022.
50 A. Broido and M. Weinstein, *Combust. Sci. Technol.*, 1970, **1**, 279–285.
51 Z. Q. Li, C. J. Lu, Z. P. Xia, Y. Zhou and Z. Luo, *Carbon*, 2007, **45**, 1686–1695.
52 M. Keiluweit, P. S. Nico, M. G. Johnson and M. Kleber, *Environ. Sci. Technol.*, 2010, **44**, 1247–1253.
53 A. C. Ferrari and J. Robertson, *Phys. Rev. B: Condens. Matter Mater. Phys.*, 2000, **61**, 14095–14107.
54 A. Cuesta, P. Dhamelincourt, J. Laureyns, A. Martinez-Alonso and J. M. D. Tascon, *Carbon*, 1994, **32**, 1523–1532.
55 J. A. Orrego Ruiz, R. Cabanzo and E. Mejìa Ospino, *Int. J. Coal Geol.*, 2011, **85**, 307–310.
56 N. E. Cooke, O. M. Fuller and R. P. Gaikwad, *Fuel*, 1986, **65**, 1254–1260.
57 G. Glover, T. J. Van Der Walt, D. Glasser, N. M. Prinsloo and D. Hildebrandt, *Fuel*, 1995, **74**, 1216–1219.
58 A. A. Salema, M. T. Afzal and F. Motasemi, *J. Anal. Appl. Pyrolysis*, 2014, **105**, 217–226.
59 J. V. Ibarra, R. Moliner and A. J. Bonet, *Fuel*, 1994, **73**, 918–924.
60 X. Fan, C. Yu, J. Yang, Z. Ling and J. Qiu, *Carbon*, 2014, **70**, 130–141.
61 M. Fan, C. Li, Y. Sun, L. Zhang, S. Zhang and X. Hu, *Sci. Total Environ.*, 2021, **799**, 149354–149365.